Flow boiling critical heat flux in a small tube for FC-72

Otsuki, Yuki
Shibahara, Makoto
Liu, Qiusheng
Sutopo, Purwono Fitri

(Citation)
Heat Transfer Research,55(9):1-16

(Issue Date)
2024-01-02

(Resource Type)
journal article

(Version)
Accepted Manuscript

(URL)
https://hdl.handle.net/20.500.14094/0100491781

Flow boiling critical heat flux in a small tube for FC-72

Yuki Otsuki[1], Makoto Shibahara[1]*, Qiusheng Liu[1], Sutopo P. Fitri[2]

[1] Graduate school of maritime sciences, Kobe University, Japan

[2] Marine Engineering Department, Institut Teknologi Sepuluh Nopember indonesia

*Correspondence: sibahara@maritime.kobe-u.ac.jp

Abstract

Flow boiling of FC-72 in a small tube was investigated experimentally. The material of the tube was SUS304 stainless steel with an inner diameter of 1.8 mm and a length of 129 mm. The effect of flow velocity and subcooling on critical heat flux (CHF) was measured in this experiment. The flow velocity, u, was varied from 0.33 to 4.26 m/s, and the inlet subcooling degree was varied from 25 to 36 K. The heat transfer coefficients from the non-boiling to boiling region were then measured. Experimental results showed that CHF increased as flow velocity was raised, but it sharply declined above u = 3.0 m/s because of premature CHF. On the basis of the experimental data, the empirical correlation between the boiling number and Weber number was obtained. The predicted value of this correlation was in agreement with the measured data within 17%.

Keywords: boiling heat transfer, heat transfer coefficient, subcooling, critical heat flux

1. Introduction

The understanding of critical heat flux (CHF) for convective boiling is important for the design and

safety assessment of power electronics in hybrid/electric/fuel cell vehicles and electric propulsion ships (Mudawar., 2011; Shibahara et al., 2018). As circuit integration of inverters and chip density of semiconductor modules increases, conventional air-cooling methods are insufficient for effective heat dissipation, making the use of liquid-cooling methods necessary. Compared to single-phase flow heat transfer, boiling heat transfer is a far more attractive method of heat dissipation because of a higher heat transfer coefficient (Bar-Cohen, 1993). Mudawar et al. concluded that in electronic chips, the heat flux must be kept close to 1 MW/m² and the surface temperature below 1131 K to maintain their performance and to ensure reliable operation (Mudawar and Maddox, 1989). Suhas and Sathyabhama, in their experiments on flow boiling of two-phase mixed fluids in rectangular channels, obtained subcooled flow boiling heat transfer coefficients (Suhas and Sathyabhama, 2017) of a water–ethanol mixture. Yu et al. obtained heat transfer coefficients in subcooled flow boiling experiments of ethylene glycol/water mixtures in a finned rectangular aluminum channel (Yu et al., 2018). The objective of their study was to elucidate the potential limitations of subcooled boiling heat transfer in power electronics cooling systems. However, the effects of subcooling degree and flow velocity on CHFs were not discussed.

The prediction of CHF at the dryout, which is the limit of heat removal by flow boiling in a small tube, has received attention in the cooling field as a complicated issue because it is strongly influenced by flow velocity and subcooling. To our knowledge, there have been few previous experimental studies for the dryout mechanism that the limit of heat removal being reached (Lee and Mudawar, 2008). Choi

et al. investigated two-phase flow boiling heat transfer in parallel microchannels of FC-72 and obtained correlations of heat transfer coefficients (Choi et al., 2017). Wong and Leong conducted flow-boiling heat transfer experiments in a closed-loop facility with a special 3D porous metal structure having unit cells with repeating spherical cavities and cylindrical connecting channels. Their visualization experiments using a high-speed camera showed that the heat transfer coefficient of FC-72 decreased at the dryout condition (Wong and Leong, 2019). Although these experiments provide insight into boiling heat transfer for FC-72, the heat removal limit in flow boiling were not discussed. Considering the above issues, we conducted flow boiling experiments in this study, using FC-72 as the working fluid and SUS304 test tubes with an inner diameter of 1.8 mm. The objective of this study is to clarify the effects of flow velocity, e-folding time, and subcooling degree on CHF.

2. Experimental setup and method

2.1 Experimental setup

The experimental setup is shown in Fig. 1. The test loop consists of a test heating element (SUS304), K-type sheathed thermocouples, pressure gauges, a cooling fan, a preheater, a temperature controller, a Coriolis flowmeter, a DC stabilized power supply, a reservoir, and a circulation pump. The liquid was allowed to flow through the reservoir into the loop, and the liquid temperature was set to 289, 293, and 298 K by a temperature controller.

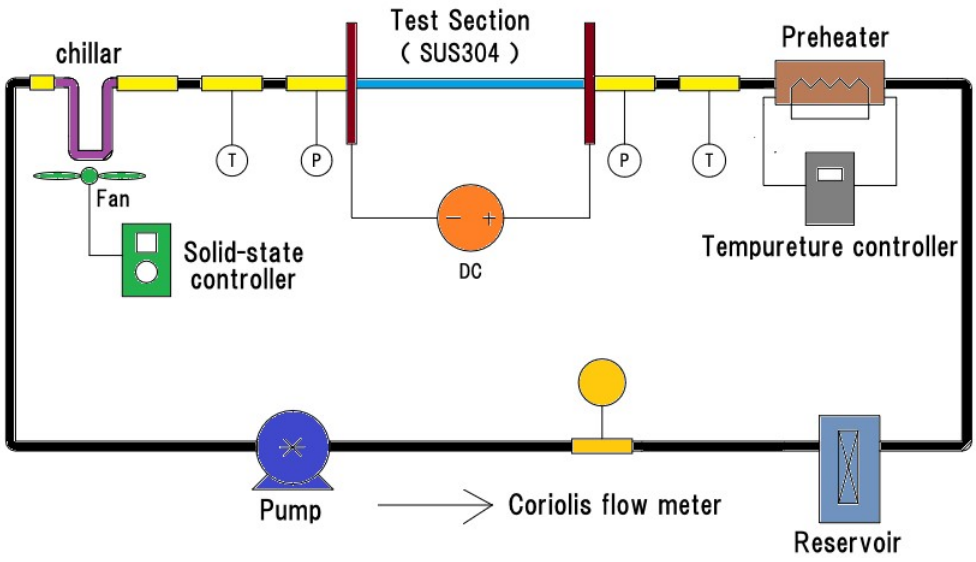

Figure 1. Schematic diagram of the water loop

Figure 2 depicts a cross-sectional view of the SUS304 test section. The inner diameter of the tube is 1.8 mm, the outlet diameter is 4.0 mm, and the heated length is 94.48 mm. Two copper plates were soldered to the tube as electrodes to provide heat through Joule heating.

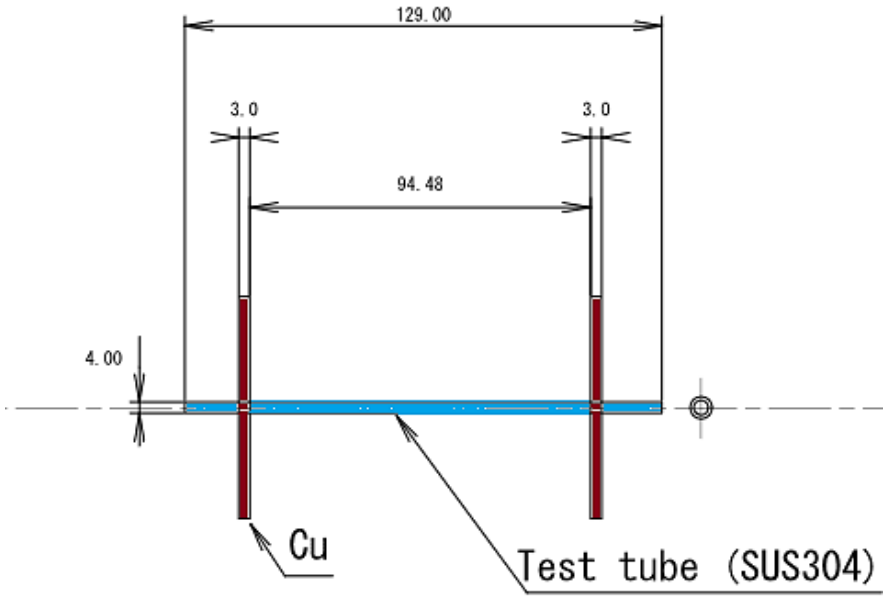

Figure 2. A cross-sectional view of the SUS304 test section

2.2 Experimental method and conditions

The experiment was conducted with the following procedure. First, the test tube was attached to the loop, and the loop was degassed using a pump to create a vacuum. Next, FC-72 was pumped from the reservoir after the flow rate and temperature had been set to the desired values, and the pressure and flow rate in the loop was stabilized. The heat input control system then applied current to the heating element in the test section, giving an exponentially increasing heating rate Q (W/m³) at various e-folding times. The heating rate is given by the following equation:

$$Q = Q_0 \exp\left(\frac{t}{\tau}\right) \tag{1}$$

where Q_0 (W/m³) is the initial heat generation rate, t (s) is time, and τ (s) is the e-folding time of the heat generation rate. Table 1 shows the experimental conditions. The boiling point of FC-72 is 329 K. The test section was placed horizontally, and the flow rate was varied from 50–650 ml/min at a flow rate interval of 50 ml/min.

Table 1. The experimental conditions

Test material	SUS304
Test liquid	FC-72
Test heating element diameter d_o (mm)	4.0
Test heating inner diameter d (mm)	1.8
Test heating element effective length L (mm)	94.48
Saturated temperature T_{sat} (K)	329
Placement direction	Horizonal
Flow rate U (ml/min)	50–650
Velocity u (m/s)	0.33–4.26
Inlet liquid temperature T_{in} (K)	289/293/298
Pressure P_{in} (kPa)	106–120
e-folding time τ (s)	1.0–20

2.3 Measurement method

The heating elements of the test section were integrated using a double-bridge circuit, shown in Fig. 3. Before each experiment was started, the heating elements were electrically equilibrated at the temperature of the test element inlet for each experiment. The unbalanced voltage V_T (V), output voltage V_I (V) of the standard resistor R_s (Ω) for current measurement, and output voltage V_R (V) of the heating element were amplified by a DC amplifier and captured as digital values in a computer via an A/D converter. The output voltages of the thermocouple for fluid temperature measurements were also amplified by a DC amplifier. The heating rate Q of the test tube was obtained from the following equations:

$$Q = V_R I \tag{2}$$

$$I = \frac{V_I}{R_S} \tag{3}$$

The electrical resistance R_T (Ω) of the test section's heating element is given by the following equations using the values of V_T and I from Ohm's law:

$$V_T = \frac{I(R_T \times R_2 - R_1 \times R_3)}{R_2 + R_3} \tag{4}$$

$$R_T = \frac{R_1 R_3 + \frac{V_T}{I}(R_3 + R_2)}{R_2} \tag{5}$$

Using R_T from Eq. (5) and the previously determined value of R_0, we calculated the average temperature of the heating element $\bar{T}$ (K) by using the following relationship:

$$R_T = R_0(1 + \alpha\bar{T} + \beta\bar{T}^2) \tag{6}$$

where, R_0 is electrical resistance at 273 K. The heat flux q (W/m^2) provided to the surface of the heating element in the test section was determined using the heating rate and the average temperature of the heating element:

$$q = \frac{V}{A}\left(Q - \rho c \frac{d\bar{T}}{dt}\right) \tag{7}$$

where, V (m^3), A (m^2), ρ (kg/m^3), and c (J/kg K) denote, respectively, the volume, surface area, density and heat capacity of the test tube. The surface temperature T_s (K) of the heating element in the test section under steady-state conditions was calculated by solving the heat conduction equation shown in Eq. (8) with the boundary condition of Eq. (9) as follows:

$$\frac{d^2T}{dr^2} + \frac{1}{r}\frac{dT}{dr} + \frac{Q}{\lambda} = 0 \tag{8}$$

$$q = -\lambda \left.\frac{dT}{dr}\right|_{r=r_i} = \frac{(r_o^2 - r_i^2)Q}{2r_i}, \quad \left.\frac{dT}{dr}\right|_{r=r_o} = 0 \tag{9}$$

$$T_s = T(r_i) = \bar{T} - \frac{qr_i}{4(r_o^2 - r_i^2)^2\lambda} \times \left[4r_o^2\left\{r_o^2(\ln r_o - \frac{1}{2}) - r_i^2(\ln r_i - \frac{1}{2})\right\} - (r_o^4 - r_i^4)\right] - \frac{qr_i}{2(r_o^2 - r_i^2)\lambda}(r_i^2 - 2r_o^2 \ln r_i) \tag{10}$$

where r_i (m) and r_o (m) are the inner and outer diameters of the heating element in the test section, respectively. λ (W/(m·K)) is the thermal conductivity of SUS304.

Estimated measurement uncertainties for the heating rate, heat flux, average temperature of the test heating element, inlet and outlet temperatures, and inlet and outlet pressures are shown in Table 2. These measurement uncertainties were calculated with ANSI/ASME PTC 19.1-1985 (ANSI/ASME, 1987).

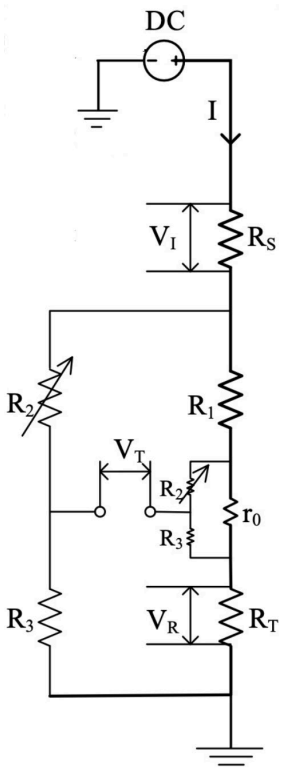

Figure 3. The double-bridge circuit used in the measurement system

Table 2. Estimated measurement uncertainties for heating value

Variables	**Equations**	**Uncertainties**
Heat generation rate	$\frac{\Delta \dot{Q}}{\dot{Q}} = \sqrt{\left(\frac{\partial \dot{Q}}{\partial V_R}\right)^2 \left(\frac{\Delta V_R}{V_R}\right)^2 + \left(\frac{\partial \dot{Q}}{\partial V_I}\right)^2 \left(\frac{\Delta V_I}{V_I}\right)^2}$	±2.0%
Heat flux	$\frac{\Delta q}{q} = \sqrt{\left(\frac{\partial q}{\partial \dot{Q}}\right)^2 \left(\frac{\Delta \dot{Q}}{\dot{Q}}\right)^2 + \left(\frac{\partial q}{\partial T_a}\right)^2 \left(\frac{\Delta T_a}{T_a}\right)^2}$	±2.4%
Inner surface temperature	$\frac{\Delta T_s}{T_s} = \sqrt{\left(\frac{\partial T_s}{\partial T_a}\right)^2 \left(\frac{\Delta T_a}{T_a}\right)^2 + \left(\frac{\partial T_s}{\partial q}\right)^2 \left(\frac{\Delta q}{q}\right)^2}$	±2.8%
Inlet and outlet temperatures	$\frac{\Delta T_{TC}}{T_{TC}} = \sqrt{\left(\frac{\partial T_{TC}}{\partial V_{TC}}\right)^2 \left(\frac{\Delta V_{TC}}{V_{TC}}\right)^2 + \left(\frac{\partial T_{TC}}{\partial V_{AMP}}\right)^2 \left(\frac{\Delta V_{AMP}}{V_{AMP}}\right)^2}$	±0.7 K
Inlet and outlet pressures	$\frac{\Delta P}{P} = \sqrt{\left(\frac{\partial P}{\partial V_P}\right)^2 \left(\frac{\Delta V_P}{V_P}\right)^2 + \left(\frac{\partial P}{\partial V_{AMP}}\right)^2 \left(\frac{\Delta V_{AMP}}{V_{AMP}}\right)^2}$	±2.6 kPa
Mass flow rate	$\frac{\Delta G}{G} = \sqrt{\left(\frac{\partial G}{\partial V_G}\right)^2 \left(\frac{\Delta V_G}{V_G}\right)^2 + \left(\frac{\partial G}{\partial V_{AMP}}\right)^2 \left(\frac{\Delta V_{AMP}}{V_{AMP}}\right)^2}$	± 0.011 kg/min

3. Experimental results

3.1 Heat transfer coefficients for FC-72

Figure 4 shows the relationship of the Reynolds and Nusselt numbers at non-boiling conditions with the solid line representing the Dittus–Boelter correlation (Dittus and Boelter, 1930) in Eq. (11). The graph shows that the Nusselt number at two different subcooling degrees increased as the Reynolds number increased, agreeing with the Dittus–Boelter correlation within 10%.

$$\mathrm{Nu} = 0.023\mathrm{Re}^{0.8}\mathrm{Pr}^{0.4} \tag{11}$$

where, Re and Pr are Ryenolds number and Prandtl number, respectively.

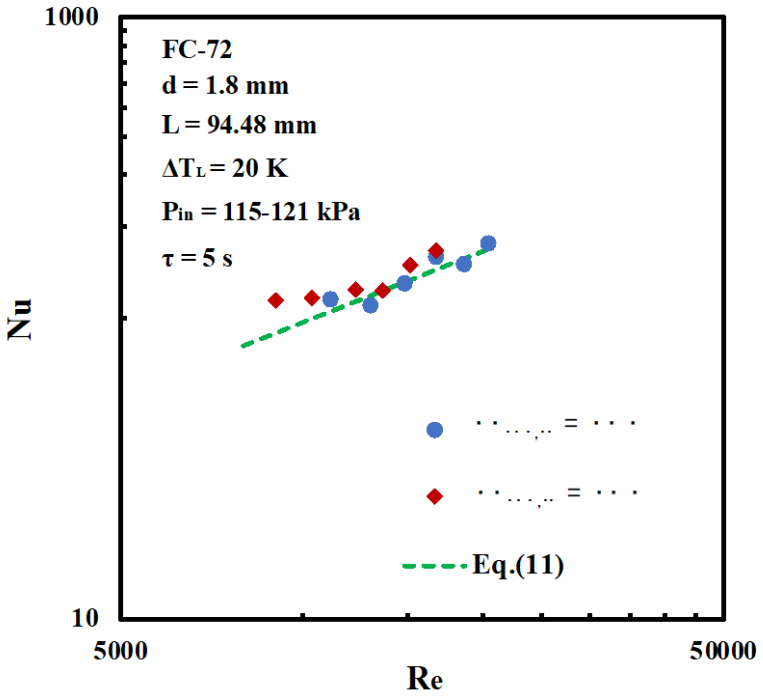

Figure 4. Relationship between Reynolds number and Nusselt number at non-boiling condition

Figure 5 shows the heat transfer coefficient with the heat flux imposed at various e-folding times. The flow velocity and the inlet subcooling were 3.0 m/s and 40 K, respectively. The heat transfer coefficient increases with heat flux. In the non-boiling region, the heat transfer coefficient is higher at shorter e-folding times (τ = 5 s) than at longer e-folding times, as shorter e-folding times lead to a thinner thermal boundary layer. At around q = 100 kW/m^2, onset of nucleate boiling (ONB) occurs, which has a different effect on the heat transfer coefficient, depending on the e-folding time. At τ = 5 s, the heat transfer coefficient decreased slightly with increasing heat flux because there is a time lag in cavity activation and occurrence of overshoot, which was not observed at τ = 10 s and higher. For all e-folding times, the heat transfer coefficient after ONB converges to nearly the same value. After reaching the point of CHF at approximately 480 kW/m^2, the heat transfer coefficient decreased drastically because of film boiling. This is because the vapor film increases thermal resistance due to the lower thermal conductivity of FC-72's vapor phase compared to its liquid phase.

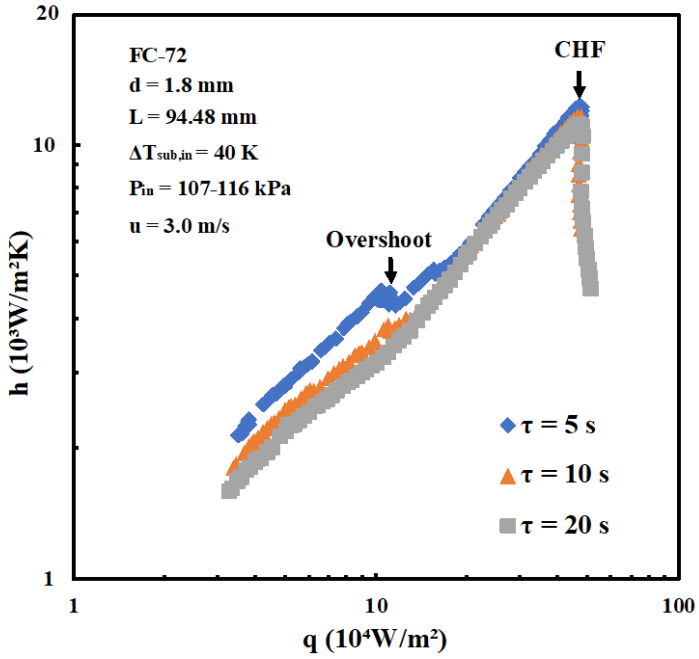

Figure 5. Heat transfer coefficient with the imposed heat flux varying from the non-boiling to the boiling region

3.2 Effect of subcooling, e-folding time, and flow velocity on boiling curves

3.2.1 Effect of degree of subcooling on boiling curve

Figure 6 depicts experimental boiling curves for three inlet subcooling ($\Delta T_{sub,in} = T_{sat} - T_{in}$): $\Delta T_{sub,in}$ = 40, 36, and 31 K at the flow velocity u = 2.3 m/s. Comparing surface superheat ($\Delta T_{sat} = T_s - T_{sat}$) at the same heat flux, the surface superheat decreases as the inlet subcooling degree increases. This can be attributed to the increase in heat transfer efficiency as the fluid inlet temperature is lowered and the increase in sensible heat required to nucleate boiling.

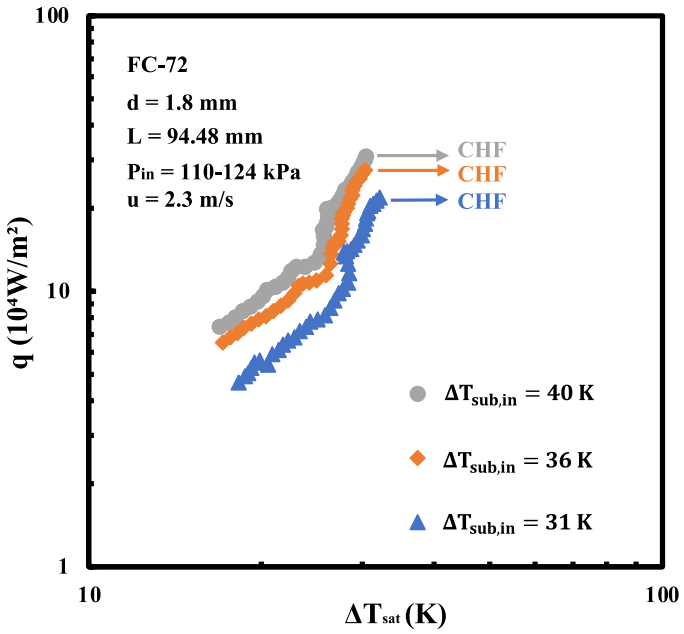

Figure 6. Boiling curve at various inlet subcooling

3.2.2 Effect of e-folding time on boiling curve

Figure 7 shows the relationship between heat flux and surface superheat at various e-folding times up to the ONB, at a flow velocity of 3.0 m/s. Four different e-folding times, τ = 1, 2, 5, and 10 s, were investigated. The results show that the heat flux increases with increasing surface superheat. Furthermore, in the region up to the ONB, the heat flux values increase as e-folding time shortens. This was attributed to the increase in heat transfer rate as the e-folding time shortens.

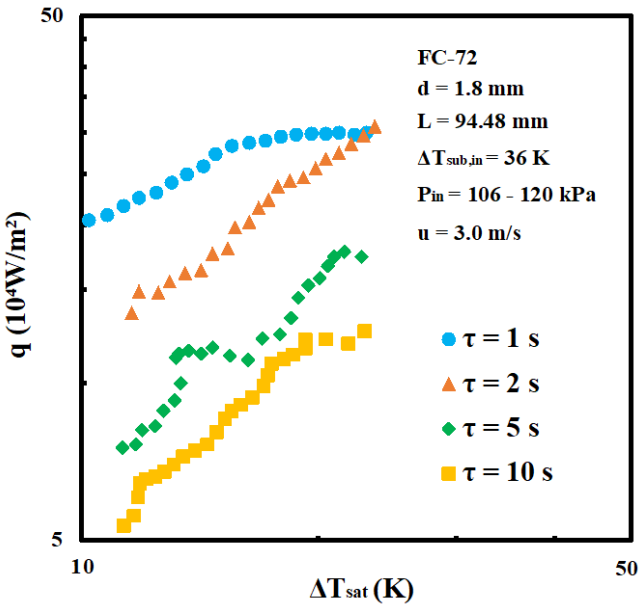

Figure 7. Relationship between heat flux and surface superheat at various e-folding times

3.2.3 Effect of flow velocity on boiling curve

Figure 8 shows the relationship between surface superheat and heat flux at different flow velocities (u = 3.0, 2.3 and 1.3 m/s) as CHF is approached. The data shows that heat flux increases with increasing flow velocity. The empirical correlation is also not consistent with that of Eq. (12), which is a formula used to predict nucleate boiling of water (McAdams et al., 1949). This disagreement is due to differences in tubes used and the physical properties of FC-72 compared to water. Rohsenow's correlation (Rohsenow, 1952), which uses FC-72 as the working fluid, correctly estimates the region of nucleate boiling at all flow velocities when setting the coefficient C_{sf} between 0.025 to 0.035 in Eq. (13).

$$\Delta T_{sat} = 22.62 q^{0.259} \tag{12}$$

$$\frac{c_{pl}\Delta T_{sat}}{h_{fg}} = C_{sf}\left(\frac{q}{\mu_l h_{fg}}\sqrt{\frac{\sigma}{g(\rho_l-\rho_g)}}\right)^{0.33}\left(\frac{c_{pl}\mu_l}{\lambda_l}\right)^{1.7} \quad (13)$$

where, c_{pl}, h_{fg}, μ_l, g and σ are specific heat, latent heat of vaporization, viscosity, acceleration of gravity and surface tension, respectively.

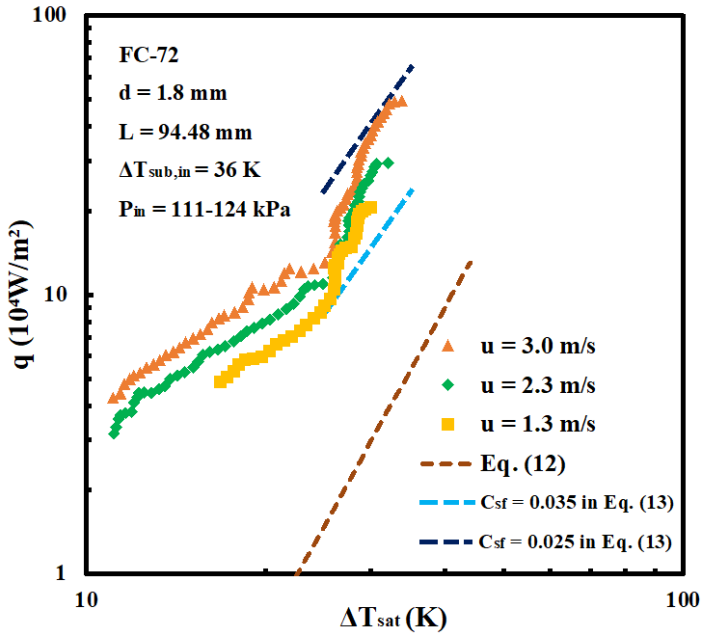

Figure 8. Boiling curve at various flow velocities with conventional correlations

3.3 Critical heat flux for FC-72

3.3.1 Effect of flow velocity on critical heat flux

Figure 9 plots the CHF for different flow velocities at the degree of subcooling of $\Delta T_{sub,in}$ = 31 K. The graph shows that the CHF increases with increasing flow velocity until the flow velocity reaches about 3.0 m/s. This can be rationalized by the following explanation: As the flow velocity increases, the shear and drag forces acting on bubbles growing on the inlet surface of the tube increase, and the

buoyancy force acting on vapor bubbles generated and released from the inlet surface of the tube decreases, causing the bubbles to rapidly detach in a short time. When the flow velocity is above 3.0 m/s, CHF decreases rapidly. This is attributed to the boiling crisis arising from the explosive-like heterogeneous spontaneous nucleation (HSN), which is exacerbated by FC-72's high wettability and low surface tension compared to water, causing it to easily fill the cavities on the heating element surface (Sutopo et al., 2010).

To confirm the descent of CHF at high flow velocity, we calculated the Departure From Nucleate Boiling Ratio (DNBR), which is the ratio of critical heat flux to local heat flux, postulated as the nucleate boiling initiation heat flux. To investigate the effect of flow velocity on the DNBR, a graph plotting flow velocity on the horizontal axis and DNBR on the vertical axis is shown in Fig. 10. DNBR increases in the region up to the flow velocity of 3.0 m/s, although not monotonically. Similar to the decrease in CHF near the flow velocity u = 3.0 m/s in Fig. 9, a sharp decrease in DNBR was observed after u = 3.0 m/s in Fig. 10. It can be concluded that premature CHF (Lee and Mudawar, 2008) with short nucleate boiling intervals occur at high flow velocity.

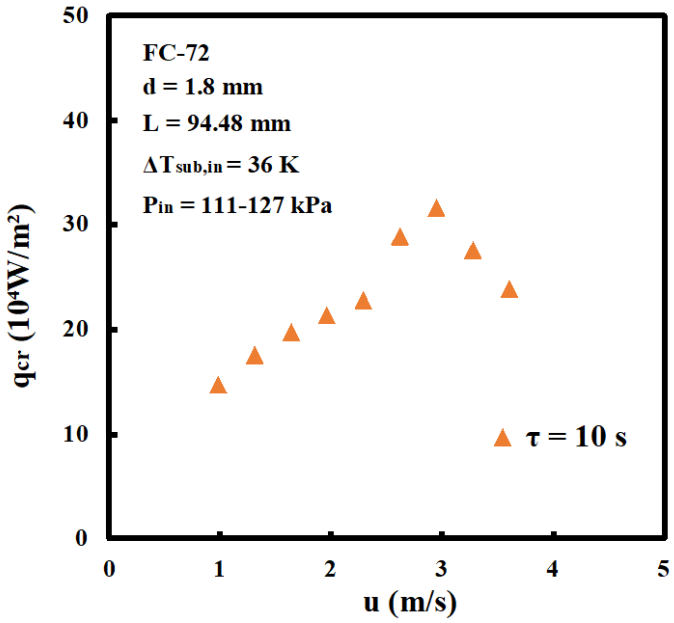

Figure 9. Effect of flow velocity on CHF

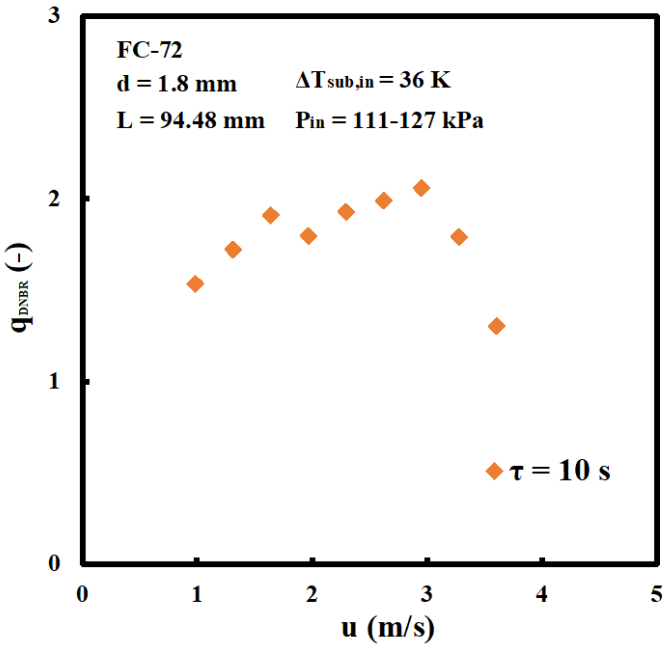

Figure 10. Effect of flow velocity on DNBR

3.3.2 Effect of subcooling on critical heat flux

Figure 11 shows the effect of inlet subcooling on CHF at various flow velocities. The inlet

subcooling degrees are 31 and 36 K. The graph shows that in the region of flow velocity less than 3.0 m/s, CHF increases as the subcooling degree increases. Above a flow velocity of 3.0 m/s, both values decrease and there is no longer a significant difference in CHF. Eq. (14) describes the relationship between CHF and flow velocity in the region of flow velocity less than 3.0 m/s.

$$q_{cr} = \{0.53u^{1.22} + 1\}\Delta T_{sub,in}{}^{0.68} \tag{14}$$

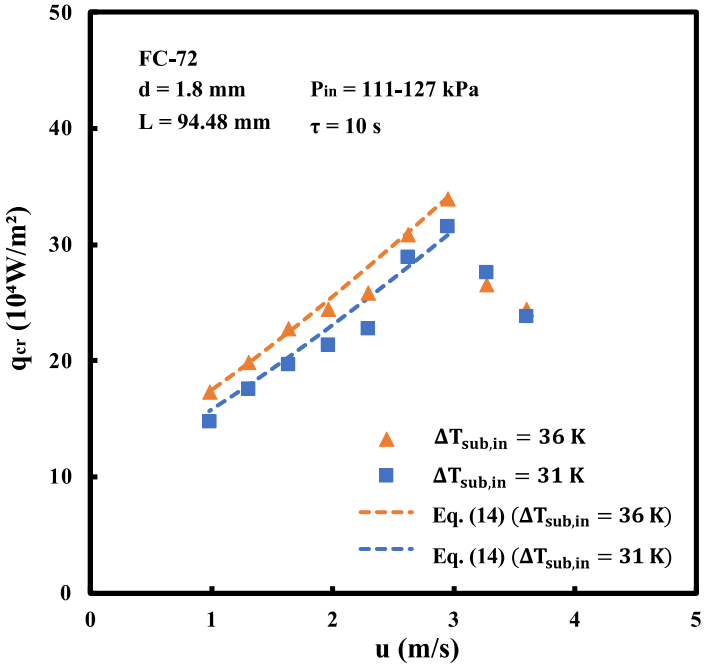

Figure 11. Effect of inlet subcooling on CHF

Figure 12 shows the effect of outlet subcooling ($\Delta T_{sub,out} = T_{sat} - T_{out,cal}$) on the CHF for each flow velocity. $T_{out,cal}$ can be calculated by the following equation as follows:

$$\boldsymbol{T_{out,cal} = T_{in} + \frac{4Lq}{uc_{pl}\rho_l d}} \tag{15}$$

where, T_{in} is the liquid temperature at the inlet of the test tube. For flow velocities less than 3.0 m/s,

CHF increases as the outlet subcooling increases. In contrast, for flow velocities above 3.0 m/s, the maximum CHF is reached around $\Delta T_{sub,out}$ = 34 K, and CHF does not increase with higher outlet subcooling. We considered this result to be the same as the decrease in CHF in the region above 3.0 m/s flow velocity in Fig. 11 due to premature CHF.

Figure 13 shows the relationship between outlet subcooling and DNBR. At flow velocities less than 3.0 m/s, the DNBR increases as outlet subcooling increases. However, above the flow velocity of 3.0 m/s, DNBR decreases around $\Delta T_{sub,out}$ = 38 K. The decrease in DNBR causes CHF at an earlier time.

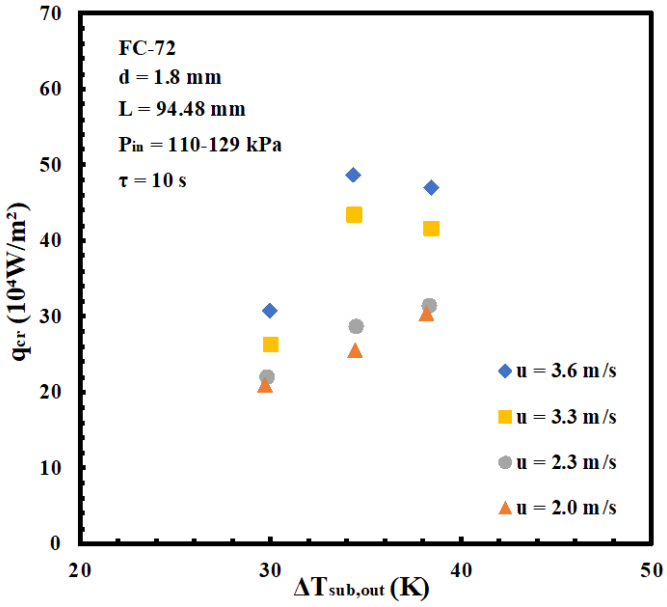

Figure 12. Effect of outlet subcooling on the critical heat flux

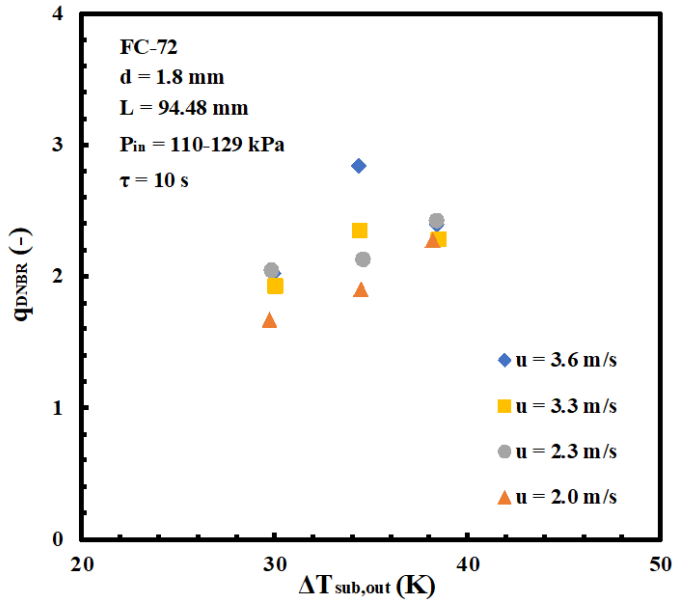

Figure 13. Effect of outlet subcooling on DNBR

3.4 Relationship between Weber number and the boiling number

Figure 14 plots the Weber number on the horizontal axis and the boiling number on the vertical axis. According to the experimental data, the boiling number decreases as the Weber number increases. The correlation was determined using Weber number We, dimensionless diameter D*, and dimensionless outlet subcooling Sc based on a previous study (Shibahara et al., 2017). The boiling number follows the Weber number with an exponent of − 0.25 as represented in Eq. (16). The predicted correlation agreed with the measured data within 17%.

$$\mathrm{Bo} = 0.0075\mathrm{We}^{-0.25}\mathrm{D}^{*-0.1}\mathrm{Sc}^{0.7} \tag{16}$$

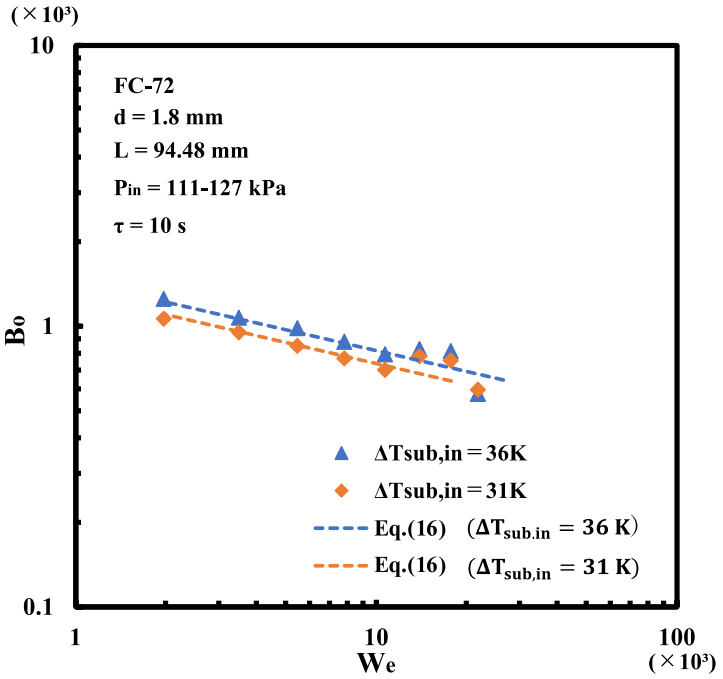

Figure 14. Relationship between boiling number and Weber number

4. Conclusions

CHFs of a flow boiling system with FC-72 as the working fluid were measured at various flow velocities and degrees of subcooling to elucidate the characteristics of boiling heat transfer, the mechanism of CHF generation, and its characteristics. The nucleate boiling of FC-72 fell between a C_{sf} of 0.025 and 0.035 in Rohsenow's correlation. It was found that for flow velocities less than 3.0 m/s, CHF values increased with increasing flow velocity and subcooling. Above the flow velocity of 3.0 m/s, CHF decreased, which was attributed to premature CHF. From the experimental data, the empirical correlation of CHF was obtained.

Acknowledgement

This work was supported by JSPS KAKENHI Grant Number JP22K04562.

Nomenclature

A	surface area, m^2
Bo	$= \frac{q_{cr}}{\rho_l u h_{fg}}$, Boiling number, (-)
c	specific heat of the test tube, J/kg K
c_{pl}	specific heat at constant pressure, J/kg K
D*	$= d/\{\sigma/g(\rho_l - \rho_g)\}^{0.5}$, non-dimensional diameter, (-)
G	mass velocity, kg/m^2s
g	acceleration of gravity, m/s^2
t	time, s
d	Inner diameter, m
h	Heat transfer coefficient, W/m^2K
h_{fg}	latent heat of vaporization, J/kg
I	Electric current, A
Nu	$= \frac{hL}{\lambda}$, Nusselt number
P	Pressure, kPa
Pr	Prandtl number

Q Heat generation rate, W/m³

q Heat flux, W/m²

R Electric resistance, Ω

R_0 Electric resistance at 273.15 K, Ω

Re $= \frac{ud}{\nu}$, Reynolds number

T_a Average temperature of the tube, K

ΔT_{sat} Surface superheat, K

ΔT_{sub} subcooling, K

T_{sat} Saturation temperature of liquid, K

u velocity, m/s

V Volume, m³

V_I Voltage, V

V_R Voltage of the standard resistor, V

We $= \frac{\rho_l L u^2}{\sigma}$, Weber number, (-)

Sc $= \frac{c_{pl}\Delta T_{sub,out}}{h_{fg}}$, non-dimensional outlet subcooling, (-)

α coefficient in Eq.(6), (-)

β coefficient in Eq.(6), (-)

ρ_l Density of liquid, kg/m³

λ Heat conductivity, W/mK

v	Kinematic viscosity, m^2/s
σ	surface tension, N/m
τ	e-folding time, s

Subscripts

AMP	Amplifier
cr	CHF
g	vapor
h	heater
i	inner
in	inlet
l	liquid
o	outer
out	outlet
s	surface
sub	subcooling
TC	thermocouple

REFERENCES

ANSI/ASME, Measurement uncertainty, supplement on instruments and apparatus", Part 1, *PTC 19.1-1985*, 1987 translated by JSME.

Bar-Cohen, A., Thermal management of electronic components with dielectric liquid, *JSME, Ser. B*, Vol. **36** Issue 1, pp.1-25, 1993.

Choi, Y. S., Lim, T. W., You, S. S., and Kim, H. S., Two-phase flow boiling heat transfer of FC-72 in parallel micro-channels, *Exp. Heat Transf.*, Vol. **30**(4), pp.284–301, 2017.

Dittus, F.W., Boelter, L.M.K., Heat Transfer in automobile radiators of the tubular type, *Int. Commun. Heat Mass Transf.*, Vol.**12**, Issue 1, pp.3-22, 1985.

Lee, J., Mudawar I., Fluid flow and heat transfer characteristics of low temperature two-phase micro-channel heat sinks – Part 1: Experimental methods and flow visualization results, *Int. J. Heat Mass Transf.*, Vol. 51, pp.4315-4326, 2008.

McAdams, W.H., Kennel, W.E., Minden, C.S., Carl, R, Picornell, P.M., Dew, J.E., Heat transfer at high rates to water with surface boiling, *Ind. Eng. Chem.*, Vol.**41**, pp.1945-1953, 1949.

Mudawar, I., Two-phase microchannel heat sinks: theory, applications, and limitations, *J. Electron. Packag.*, Vol. **133**, pp.41002, 2011.

Maddox, D.E. and Mudawar, I., Critical Heat Flux in Subcooled Flow Boiling of Fluorocarbon Liquid on a Simulated Electronic Chip in a Rectangular Channel, *Int. J. Heat Mass Transf.*, Vol. **32**, pp. 379-394, 1989.

Rohsenow, W. M., A Method for Correlating Heat-Transfer Data for Surface Boiling of Liquids, *Transactions of ASME*, vol.74, pp.969–976, 1952.

Shibahara, M., Fukuda, K., Liu, Q.S., and Hata, K., Prediction of forced convective heat transfer and critical heat flux for subcooled water flowing in miniature tubes, *Heat Mass Transf.*, Vol. **54**(2), pp.501–508, 2018.

Shibahara, M., Liu, Q.S., Hata, K.. and Fukuda, K.. Boiling heat transfer and CHF for subcooled water flowing in a narrow channel due to power transients, *Exp. Heat Transf.*, Vol.**33**(1), pp.64-80, 2020.

Shibahara, M. Fukuda, K., Liu, Q.S., and Hata, K., Correlation of high critical heat flux during flow boiling for water in a small tube at various subcooled conditions, *Int. Commun. In Heat and Mass Transfer,* Vol. 82, pp.74-80, 2017.

Suhas, B. G. and Sathyabhama, A., Heat transfer and force balance approaches in bubble dynamic study during

subcooled flow boiling of water-ethanol mixture, *Exp. Heat Transf.*, Vol. **31**(1), pp.1–21, 2018.

Sutopo, P.F., Fukuda, K., Liu, Q.S., Direct Transition Phenomena in Pool Boiling of FC-72, *J. Therm. Sci. Tech*. Vol. **5**(2)**,** pp.206-221, 2010.

Wong, K.K., Leong., K.C., Nucleate flow boiling enhancement on engineered three-dimensional porous metallic structures in FC-72, *Appl. Therm. Eng. 159*, 113846, 2019.

Yu, W., France, D. M., Singh, D., and Zhao, W., Experimental investigation of subcooled flow boiling of a 50/50 ethylene glycol/water mixture in finned rectangular aluminium channels, *Exp. Heat Transf.*,

vol. **31**(6), pp.482–494, 2018.